Directional porin binding of intrinsically disordered protein sequences promotes colicin epitope display in the bacterial periplasm

Nicholas G. Housden[1], Patrice Rassam[1,†], Sejeong Lee[2], Firdaus Samsudin[3], Renata Kaminska[1], Connor Sharp[1], Jonathan D. Goult[1], Marie-Louise Francis[1], Syma Khalid[3], Hagan Bayley[2] and Colin Kleanthous[1]*

[1]*Department of Biochemistry, University of Oxford, South Parks Road, Oxford OX1 3QU, UK*

[2]*Department of Chemistry, University of Oxford, 12 Mansfield Road, Oxford OX1 3TA, UK*

[3]*Department of Chemistry, University of Southampton, University Road, Southampton SO17 1BJ, UK*

*To whom correspondence should be addressed:

colin.kleanthous@bioch.ox.ac.uk; Telephone: +44-1865-613370; Fax: +44-1865-612313

ABSTRACT: Protein bacteriocins are potent narrow spectrum antibiotics that exploit outer membrane porins to kill bacteria by poorly understood mechanisms. Here, we determine how colicins, bacteriocins specific for *Escherichia coli*, engage the trimeric porin OmpF to initiate toxin entry. The N-terminal ~80 residues of the nuclease colicin ColE9 are intrinsically unstructured and house two OmpF binding sites (OBS1 and OBS2) that reside within the pores of OmpF and which flank an epitope that binds periplasmic TolB. Using a combination of molecular dynamics simulations, chemical trimerization, isothermal titration calorimetry, fluorescence microscopy and single channel recording planar lipid bilayer measurements, we show that this arrangement is achieved by OBS2 binding from the extracellular face of OmpF, whilst the interaction of OBS1 occurs from the periplasmic face of OmpF. Our study shows how the narrow pores of oligomeric porins are exploited by colicin disordered regions for direction-specific binding, which ensures the constrained presentation of an activating signal within the bacterial periplasm.

KEYWORDS Bacteria, outer membrane, colicin, intrinsic disorder, porin, OmpF, tridentate ligand

INTRODUCTION

The asymmetric Gram-negative outer membrane (OM) is a robust protective barrier blocking entry of both hydrophilic and hydrophobic compounds into bacteria. As a result, and in order to obtain nutrients and exchange metabolites, bacteria incorporate thousands of multimeric porins in the OM, the narrow pores of which act as size and chemical selectivity filters that simultaneously exclude toxic compounds such as bile salts(*1*). Porins are also the route by which major classes of antibiotics such as β-lactams enter bacteria whereas other, much larger, antibiotics such as vancomycin are excluded(*2*). Notwithstanding the size selective nature of these pores bacteria have evolved competitive strategies to exploit porins to deliver bacteriocins(*3*). Bacteriocins play prominent roles in shaping bacterial communities and are implicated in the killing of commensal bacteria during pathogen invasion of hosts(*4-6*). Protein bacteriocins, typified by colicins that target *Escherichia coli*, are orders-of-magnitude larger than the size selectivity filters of porins yet are still able to enter and kill bacteria. Previous work on the endonuclease (DNase) colicin ColE9 has shown that cell entry is initiated by its intrinsically unstructured translocation domain (IUTD), which penetrates the narrow pores of porins(*7, 8*). Using *in silico*, *in vitro* and *in vivo* approaches we show how directional binding by ColE9's IUTD ensures its activating Tol binding epitope (TBE) is presented appropriately in the bacterial periplasm.

Nuclease bacteriocins target DNA, rRNA or tRNAs and are widely distributed amongst γ-proteobacteria, particularly the pathogens *Escherichia coli, Pseudomonas aeruginosa, Klebsiella pneumoniae, Shigella sonnei and Serratia marcescens(6)*. Sequence surveys of thousands of such bacteriocins suggests they often have intrinsically disordered sequences at their N-termini(*6*). ColE9 uses its disordered sequence to engage the periplasmic Tol-Pal system, which is coupled to the proton-motive force (PMF) across the inner membrane (IM), via OmpF(*9*). Specifically, ColE9 assembles an OM translocon that includes BtuB, its receptor, OmpF, its translocator, TolB, its periplasmic target, and Im9, its immunity protein(*8*). Im9 binds and neutralizes the DNase of ColE9 with fM affinity in the producing host cell(*10*) and is displaced at the surface of a susceptible cell in a force-dependent manner(*11*). This force is provided by the PMF and transduced to the translocon by TolA in conjunction with its IM protein partners, TolQ and TolR.

ColE9's OmpF binding sites (OBSs) bind with micromolar affinity to the narrow lumen of OmpF subunits, which are only wide enough to accommodate unfolded polypeptides. While neither is essential removal of both abolishes ColE9 toxicity(*7*). Residues 2-18 (SGGDGRGHNTGAHSTSG) comprise OBS1 (colicins usually lack an N-terminal methionine) and OBS2 comprises residues 54-63 (IHWGGGSGRG). Both OBSs bind detergent solubilised OmpF as isolated peptides in ITC experiments, exhibiting equilibrium dissociation constants (K_ds) of 2 and 24 μM, respectively, at pH 6.5 and at 25°C,

and with stoichiometries of ~3 peptides/OmpF trimer(7). A crystal structure of ColE9 OBS1 bound to OmpF confirms its location within the lumen, but the low resolution of the structure and that of ColE3 IUTD bound to OmpF has left the question of peptide orientation unanswered(*7, 12*). In a purified BtuB·ColE9·OmpF·TolB translocon complex, two pores of an OmpF trimer are occupied by a single colicin molecule(*8*). For this to occur and the TolB-binding epitope to be correctly presented in the periplasm would require binding of OBS1 from the periplasmic face of OmpF (Figure 1). We therefore set out to determine if OBS sequences show directional binding to the luminal pores of OmpF.

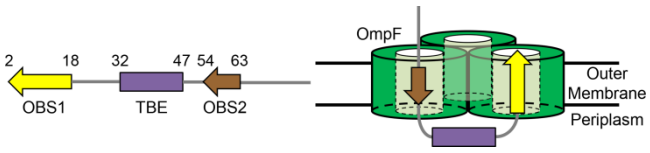

Figure 1. ColE9 IUTD with the TBE flanked by OBS1 and OBS2. Binding of two OBSs to OmpF presents the TBE in the periplasm(*8*). OBSs represented with arrowheads at N-termini to highlight direction of binding.

EXPERIMENTAL SECTION

Expression and Purification

The construction of pNGH027 and pNGH068 encoding ColE9$^{1-32}$-DNase·Im9 and ColE9$^{53-83}$-DNase·Im9 in pET21a (Novagen) has previously been described elsewhere(7). Whole plasmid mutagenesis was used to insert T25C and S71C single cysteine mutations into pNGH027 and pNGH068 respectively to give pNGH078 and pNGH079. The D5A mutation and Δ2-5 deletion were introduced into pNGH078 yielding pNGH216 and pNGH210 respectively. ColE9$^{1-32}$-DNase, T25C ColE9$^{1-32}$-DNase, Δ2-5 ColE9$^{1-32}$-DNase, D5A ColE9$^{1-32}$-DNase, ColE9$^{53-83}$-DNase and S71C ColE9$^{53-83}$-DNase were expressed in BL21 (DE3) cells and purified as previously described by nickel affinity chromatography followed by size exclusion chromatography(7).

OmpF was purified from B^{E}3000 using a protocol modified from Housden et al(*8*). Briefly, cultures of B^{E}3000 cells were grown in M9 minimal media in the presence of 0.4 % (w/v) glucose, 0.1 % (w/v) casamino acids, 3 μg/ml $FeCl_3$, for 6 hours at 37 °C, before harvesting by centrifugation. Cells were lysed through sonication and outer membranes purified as previously described, before extracting OmpF in 10 mM Tris-HCl, pH 8.0, 2 % (w/v) n-octyl-β-D-glucopyranoside, 5 mM EDTA. Homogeneous OmpF was obtained through three chromatographic steps, initially with a disposable 5 ml Q-

Sepharose column (GE Healthcare), which removed the majority of the associated LPS from OmpF, followed by size exclusion chromatography using a 16/60 Sephacryl 300 HR column (GE Healthcare), before a final anion chromatography step on a MonoQ 4.6/100 PE column (GE Healthcare). All three columns were equilibrated in 25 mM Tris-HCl, pH 8.0, 5 mM EDTA, and 1 % (w/v) n-octyl-β-D-glucopyranoside and bound proteins were eluted from the anion exchange columns using a 0 to 500 mM LiCl gradient.

TMR labelling

Labelling of Im9 was performed using C23A, E58C Im9, where the native cysteine which has poor accessibility for labelling is removed and a surface exposed cysteine is introduced. C23A, E58C Im9 was reduced with 5 mM DTT and buffer exchanged into 50 mM potassium phosphate, pH 7.0, 100 mM NaCl with a 5 ml HiTrap desalting column (GE Healthcare), before adding a 5-fold molar excess of TMR (Sigma-Aldrich) and incubating at 4 °C for 1 hour. The labelling reaction was quenched through the addition of 5 mM DTT and excess fluorophore removed using a 5 ml HiTrap desalting column.

TMEA conjugation

T25C ColE9$^{1-32}$-DNase and S71C ColE9$^{53-83}$-DNase were purified by nickel affinity chromatography eluting with 6 M GdnHCl to give OBS-E9 DNase in the absence of immunity protein. Following refolding by dialysis into 25 mM Tris-HCl, pH 7.5, 150 mM NaCl samples were reduced through addition of DTT to a final concentration of 10 mM. 10 ml aliquots of protein at a concentration of 100 μM were loaded onto a HiPrep 26/60 Superdex 75 column equilibrated in 25 mM Tris-HCl, pH 7.5, 150 mM NaCl in the absence of reductant. Monomeric protein was pooled and quantified through $A_{280\ nm}$ (using sequence based extinction coefficient of ε280 nm = 16,960 $M^{-1}.cm^{-1}$ and ε280 nm = 22,460 $M^{-1}.cm^{-1}$ for T25C ColE9$^{1-32}$-DNase and S71C ColE9$^{53-83}$-DNase respectively) and TMEA (Thermo Fisher Scientific) was added at a molar ratio of three proteins per TMEA. Following 2-hour incubation at 22 °C, DTT was added to a final concentration of 5 mM and $(OBS)_3$ was separated from $(OBS)_2$ and OBS through size exclusion chromatography on a 26/60 Superdex 75 column. For fluorescence microscopy C23A E58C^{TMR} Im9 was added in a 1.3-fold molar excess over E9 DNase, with excess free immunity removed by gel filtration on a Superdex 75 column.

Molecular dynamics simulations

The structure of OmpF trimer (PDB: 2OMF) embedded within a DPPC membrane was obtained from the MemProt MD database(*13*). Structures of OBS1 and OBS2 peptides were generated using PyMOL(*14*). The OBS peptide was placed in bulk solution approximately 5 nm above one OmpF subunit on the extracellular side. Steered MD simulations were performed whereby a harmonic spring was attached to the N-terminus of the OBS peptide and pulled at a constant velocity of 0.01 $nm.ps^{-1}$. The peptide was pulled through the OmpF pore into the periplasmic space until the distance between their centres of mass was around 10 nm. Using similar parameters, the OBS peptides were pulled in the opposite direction from the periplasmic space into the extracellular side through the OmpF pore. Each steered MD simulation was repeated three times starting with different initial velocities and an average of force required to pull the peptide from three independent simulations was calculated. Simulations were performed at neutral conditions, 150 mM NaCl at a temperature of 310 K.

The structure of ColE9 OBS1 peptide from Housden et al(*7*) was docked onto OmpF Trimer (PDB: 2OMF) embedded within a DPPC membrane. Missing atoms were added using PyMOL. The structure of the peptide in reverse orientation was manually built using a text editor based on the positions of the peptide backbone in the crystal structure, and the side chains were later added using PyMOL. All systems underwent a 10-ns equilibration simulation with positional restraints applied to the heavy atoms of the protein and peptide. These restraints were removed during subsequent 100 ns production simulation, which were performed in triplicate.

Isothermal Titration Calorimetry

ITC measurements were performed on a MicroCal iTC_{200} thermostated at 25 °C with all proteins prepared in 20 mM potassium phosphate buffer pH 6.5, 1 % (w/v) β-OG. OmpF was present in the sample cell at concentrations of 4-11 μM with ligand concentration in the syringe between 120 and 375 μM depending on the affinity of the interaction. To allow comparison between monomeric and trimeric ligands, the concentration of all ligands was specified in terms of molarity of binding epitopes. After an initial injection of 0.5 μl, 19 aliquots of 2 μl were injected, with a spacing of 180 seconds between each injection. For each titration, a control titration of ligand into buffer was performed. After subtraction of the heats of dilution data were fitted to a single set of identical sites binding model using the manufacturer's software.

Microscopy

50 μl overnight *E. coli* culture was inoculated into 4 ml of M9-Glucose minimal media (2 mM $MgSO_4$, 0.1 mM $CaCl_2$, 0.1 mM $FeSO_4$, 1g/L NH_4Cl, 0.4 % (w/v) glucose, 0.05 % (w/v) casamino acids) and grown until OD600~0.4. 200 μl cells were

pelleted by centrifugation (7000 g, 3 minutes) and resuspended in PBS. Cells were pelleted and fixed in 200 µl 4 % para-formaldyhyde (PFA) solution for 10 minutes with mixing by rotary inversion, before another PBS wash. Fixed cells were permeabilised through resuspension in either 0.1 % (v/v) Tween-20 or Triton X-100, incubated for 10 min at room temperature, before pelleting and washing with PBS. Labelling was performed through resuspension of the cell pellet in 50 µl PBS containing 1 µM fluorescently labelled OBS^{TMR} construct. After 15 minutes incubation at room temperature with rotary inversion, cells were washed by pelleting (7000 g, 3 minutes) and resuspension in PBS solution, prior to mounting cells between an agar pad and a coverslip. The agar pad was made with 200 µl of M9 containing 1 % UltraPure^{TM}agarose (w/v), introduced into a 1.5 cm × 1.6 cm Gene Frame matrix (Thermo Fischer Scientific) that was previously adhered to a clean slide. The agar pad was formed by addition of a clean coverslip on top until solidification had occurred. 10 µl of stained bacteria was added to the pad, which was sealed afterward using a clean coverslip. Measurements were taken using a Zeiss LSM 780/Axio Examiner Z1 motorised upright laser scanning microscope equipped with DIC for bright field and HeNe 561nm laser (1 mW) for red channel. Optical magnification was provided by a 100x oil-immersion objective (Zeiss, NA 1.4). Images were recorded by scanning the laser over a 13.5 µm x 13.5 µm area with the image size set to 512 pixels x 512 pixels, scan speed set to 7 (3.15 µs/pixel) and a digital zoom of 10x. Images were recorded using Zeiss Zen 2011 software. Image processing and intensity quantification was obtained using ImageJ. A mask delimiting the contour of each cell was applied and the mean intensity was determined after normalizing with background fluorescence.

Single-channel recordings in planar lipid bilayers

Planar lipid bilayers were formed by using a solution of 1,2-diphytanoyl-sn-glycerol-3-phosphocholine (DPhPC) (Avanti Polar Lipids, Alabaster, AL, USA) dissolved in pentane (5 mg ml^{-1}) across a 100 µm diameter aperture in a 25 µm thick Teflon film(*15*). Currents were recorded by using a patch clamp amplifier (Axopatch 200B, Axon Instruments, Foster City, CA, USA) with a sampling interval of 100 µs (10 kHz acquiring frequency). Data were filtered with a 2 kHz low-pass Bessel filter and digitised with a Digidata 1322 A converter (Axon Instruments) at a sampling frequency of 10 kHz. Data analysis was performed with pClamp 10.3 software (Molecular Devices).

OmpF trimer (0.5 µl of 33.7 µM or 0.2 µl of 66 µM protein in 20 mM Tris-HCl, pH 8.0, 5 mM EDTA, 50 mM LiCl, 1 % (w/v) β-OG) was added to the *cis* compartment (at ground) and incubated until a single porin had inserted into the bilayer. Currents were recorded after the *cis* chamber had been perfused with 20 mM potassium phosphate, pH 6.5, 100 mM KCl, to remove excess protein. Both the *cis* and *trans* compartments of the apparatus contained 20 mM potassium phosphate pH 6.5, 100 mM KCl, (1 ml), at 20.5 ± 0.5 °C.

Before adding the $(OBS)_3$ constructs to either side of OmpF, the orientation of OmpF in the bilayers was defined by using an I-V curve plot(*16*). With the defined positive-asymmetry of OmpF, the binding of $(OBS)_3$ constructs to the extracellular side was monitored by adding the construct (50 nM) into the *cis* compartment at a holding potential of – 100 mV. The binding of the $(OBS)_3$ constructs to the periplasmic side OmpF was monitored by adding the construct (50 nM) into the *trans* compartment at a holding potential of + 100 mV. When the negative-asymmetry of OmpF was defined, measurements were carried out the opposite way.

RESULTS AND DISCUSSION

Directionality of OBS binding was initially addressed through steered MD simulations. Simulations were conducted whereby a harmonic spring was attached to the N-terminus of each OBS peptide and pulled through OmpF embedded in a dipalmitoylphosphatidylcholine (DPPC) membrane. Steered MD simulations were performed both for OBS1 and OBS2, pulling each peptide from the extracellular side of OmpF into the periplasm and from the periplasm to the extracellular side of OmpF, with the average force required to pull the peptide calculated from three independent simulations (**Supplementary Figure 1**). Simulations with OBS2 showed a force of 119 $kcal.mol^{-1}.nm^{-1}$, was required to pull the peptide through OmpF in either direction, whilst equivalent simulations with OBS1 showed a directional bias. To pull OBS1 from the extracellular space into the periplasm required a force of 119 $kcal.mol^{-1}.nm^{-1}$, whereas passage in the opposite direction required a force of 143 $kcal.mol^{-1}.nm^{-1}$, with the difference potentially attributable to overcoming the binding interaction OBS1 with OmpF in the periplasmic-to-extracellular orientation.

Given the apparent preference of OBS1 for OmpF binding from the periplasmic side of the porin we performed further MD simulations of this complex using OmpF embedded in a DPPC membrane. Simulations with the N-terminus facing the periplasm (the orientation originally ascribed to OBS1 in the crystal structure of OmpF-OBS1 complex) showed the peptide did not stably bind the pore, with residues 2 to 8 showing a high degree of mobility. These residues detached from the original position within the first few nanoseconds and bound to several other residues in the pore, but did not reach a stable conformation within the timeframe of the simulation (100 ns). In contrast, the C-terminus of the peptide, positioned in the constriction zone of the OmpF pore, remained bound to OmpF throughout, preventing release of the peptide into the periplasm. In equivalent simulations with the N-terminus facing the extracellular face of OmpF, motion of the N-terminus of the peptide was limited by the constriction of the pore. The C-terminus, positioned in the wider

periplasmic face of the pore was more mobile but remained bound to its original position for the majority of the simulation. As a result, the entire OBS1 peptide bound OmpF more stably, oriented with its N-terminus facing the extracellular face of OmpF. In summary, MD simulations suggest OBS1 binds preferentially from the periplasmic side of the porin, consistent with the N-terminus of the colicin translocating entirely through OmpF in order to approach its optimal binding position from the periplasm.

In order to probe directionality of each OBS *in vivo* we developed a microscopy platform that would allow labelling of OmpF-expressing cells with fluorescently-labelled OBS derivatives. Our strategy was based on previously described OBS fusions(*7*), which can subsequently be labelled with fluorophores. The fusion protein in each case was the colicin E9 DNase domain itself; the domain not only expresses to high yield but can be readily labelled non-covalently with fluorescently-labelled Im9 (see Experimental Section). ColE9$^{1-32}$-DNase and ColE9$^{53-83}$-DNase, which have OBS1 and OBS2, respectively, at the N-terminus bind OmpF in ITC experiments albeit ColE9$^{53-83}$-DNase binds 5-fold weaker than the OBS2 peptide(*7*). We bound Im9, pre-labelled with tetramethyl rhodamine (TMR), to the DNase domain fusions. Im9 binds the ColE9 DNase with a K_d of 10^{-14} M(*10*). The heterocomplexes, referred to as OBS1^{TMR} and OBS2^{TMR}, were then used to label OmpF-expressing cells in confocal fluorescence microscopy experiments (**Supplementary Figure 2**). We observed only weak labelling of B^{E}3000 cells expressing OmpF as the predominant porin, even when the cells were permeabilised by pre-treatment with Tween-20 to expose the bacterial periplasm.

We rationalised that the weak labelling of OmpF-expressing cells observed for each OBS fusion was likely due to the micromolar binding of single OBS sequences for an OmpF subunit. Preparation of fluorescently-labelled cells with exogenous fluorophores (e.g.(*17*)) typically involves multiple wash steps to remove non-specifically bound fluorophore. In order to increase the affinity of these labels for OmpF through avidity, and so minimise loss of label during washing, we generated tridentate OBS constructs. First, single cysteine mutants of each OBS fusion (T25C ColE9$^{2-32}$-DNase and S71C ColE9$^{53-83}$-DNase, respectively) were generated where the cysteine was placed outside of the OBS. Tridentate versions were prepared by reaction with tris(2-maleimidoethyl)amine (TMEA), a trifunctional crosslinker with three reactive maleimide groups. The resulting tridentate OBS constructs were purified by size exclusion chromatography (**Supplementary Figure 3**) and their binding to OmpF investigated through ITC. The tridentate constructs $(OBS1)_3$ and $(OBS2)_3$ bound OmpF stoichiometrically with K_ds of 28 nM and 480 nM, respectively, two orders-of-magnitude tighter than their monomeric counterparts (**Figure 2**). For $(OBS1)_3$, formation of the tridentate ligand had little impact on the thermody-

namics of binding. For $(OBS2)_3$, trimerisation had a detrimental impact on enthalpy but this was compensated by a reduction in the entropic penalty of binding.

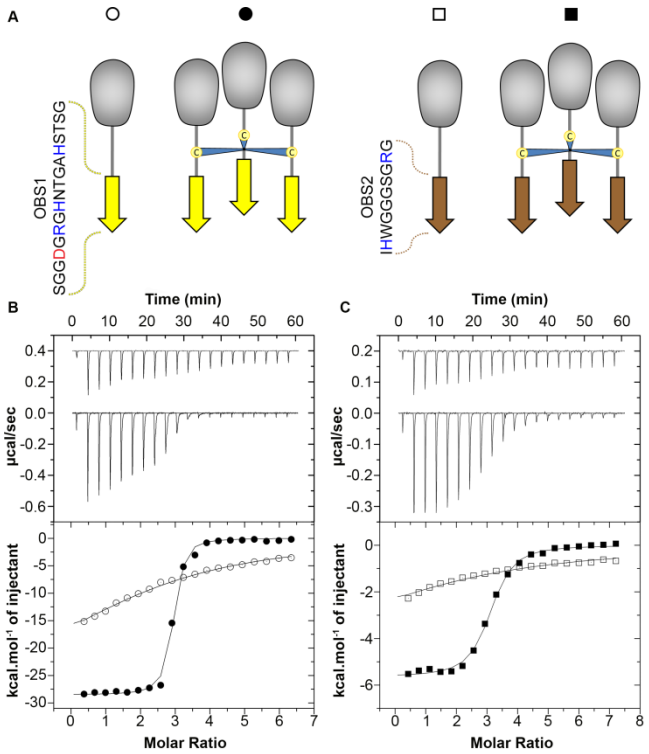

Figure 2. TMEA mediated trimerization of T25C ColE9$^{1-32}$-DNase (OBS1) and S71C ColE9$^{53-83}$-DNase (OBS2) yields high affinity tridentate OmpF ligands. **(A)** Cartoon representation of OBS DNase fusion proteins in their monomeric and tridentate forms. Sequences of OBS1 and OBS2 represented by yellow and brown arrows, respectively, are shown. **(B)** Titration of 120 µM OBS1 (○) and 40 µM $(OBS1)_3$ (●) into 4 µM OmpF trimer, in 20 mM potassium phosphate buffer, pH 6.5, 1 % (w/v) β-OG. When fitted to a single set of identical sites binding model the tridentate complex gives a K_d of 29 ± 2 nM, N = 3.0 ± 0.3 and ΔH = -26.7 ± 2.1 kcal.mol^{-1}, compared to the previously published values of K_d = 2.5 µM, N = 2.5 and ΔH = -26.7 kcal.mol^{-1} for the binding of OBS1 to OmpF under identical conditions(7). **(C)** Titration of 375 µM OBS2 (□) and 125 µM $(OBS2)_3$ (■) into 11 µM OmpF trimer, in 20 mM potassium phosphate buffer, pH 6.5, 1 % (w/v) β-OG. Data were fitted to a single set of identical sites binding model to give K_d = 480 ± 5 nM, N = 3.0 ± 0.1 and ΔH = -5.64 ± 0.01 kcal.mol^{-1}, compared to previously published values of K_d = 134 µM, N = 2.6 and ΔH = -27.6 kcal.mol^{-1} for the binding of OBS2 under identical conditions(7).

Each tridentate was made fluorescent by the addition of TMR-labelled Im9 to generate $(OBS1)_3^{TMR}$ and $(OBS2)_3^{TMR}$, added to B^E3000 cells and cells imaged by confocal fluorescence microscopy (**Figure 3 and Supporting Figure 4**). $(OBS1)_3^{TMR}$ failed to label cells whilst $(OBS2)_3^{TMR}$ under equivalent conditions labelled the cells, suggesting OBS2 binds stably from the extracellular medium while OBS1 cannot. To determine if OBS1 is able to bind OmpF-expressing cells from the

periplasm we first permeabilised B^E3000 cells, either by the addition of Tween-20 or Triton X-100. Now, strong cell labelling was observed with $(OBS1)_3^{TMR}$, indicating that OBS1 binding to OmpF requires access to its binding site from the periplasmic face of OmpF. To verify that the observed labelling was due to specific interaction with OmpF, experiments were repeated using BZB1107 cells, a derivative of B^E3000 cells where *ompF* is inactivated with a kanamycin cassette. No labelling was seen in these cells for $(OBS1)_3^{TMR}$ or $(OBS2)_3^{TMR}$ even with permeabilisation of the outer membrane (**Figure 3**).

Addition of unlabelled $(OBS1)_3$ to permeabilised cells prevented subsequent labelling with $(OBS2)_3^{TMR}$ whilst addition of $(OBS2)_3$ before $(OBS1)_3^{TMR}$ also prevented labelling of cells. In the absence of permeabilisation, addition of $(OBS1)_3$ had no impact on $(OBS2)_3^{TMR}$ labelling (data not shown). These observations are consistent with OBS1 binding from the periplasmic face of OmpF whilst OBS2 binds from the extracellular face, and, as previously observed by ITC(7), the binding sites for OBS1 and OBS2 overlap, which prevents simultaneous binding to the same OmpF subunit.

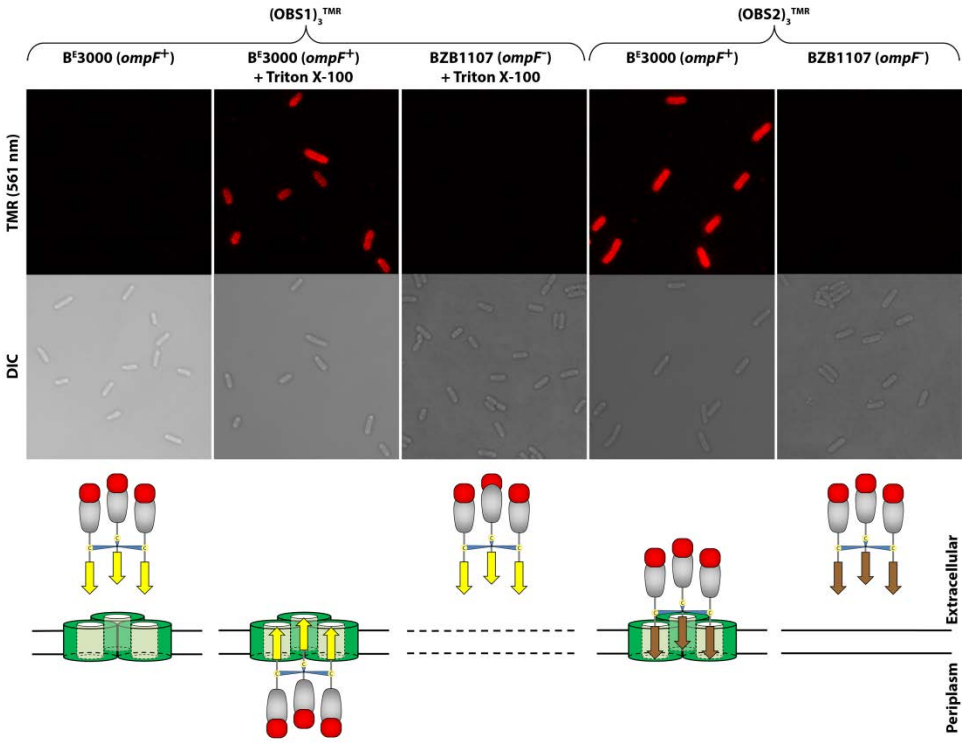

Figure 3. Confocal microscopy data showing tridentate OBS1 binds OmpF from the periplasm while tridentate OBS2 binds from the extracellular medium. $(OBS1)_3^{TMR}$ only bound to OmpF when *E. coli* B^E3000 cells were permeabilised (compare columns 1 and 2), whereas $(OBS2)_3^{TMR}$ could bind intact cells (column 4), suggesting the two OBSs associate with OmpF in opposite directions. No staining of BZB1107 *ompF*- cells was observed in the presence of either $(OBS1)_3^{TMR}$ or $(OBS2)_3^{TMR}$, even when cells

where permeabilised. Ligands were added to mid-log cultures of B^E3000 and BZB1107 cells. Following extensive washing, cells were mounted between an agar pad and a coverslip for imaging. Imaging was carried out on at least 3 regions of interest (21 µm x 21 µm) per condition. n = 30 cells in each experiment. Quantification of the fluorescence intensities is shown in Supplementary Figure 4.

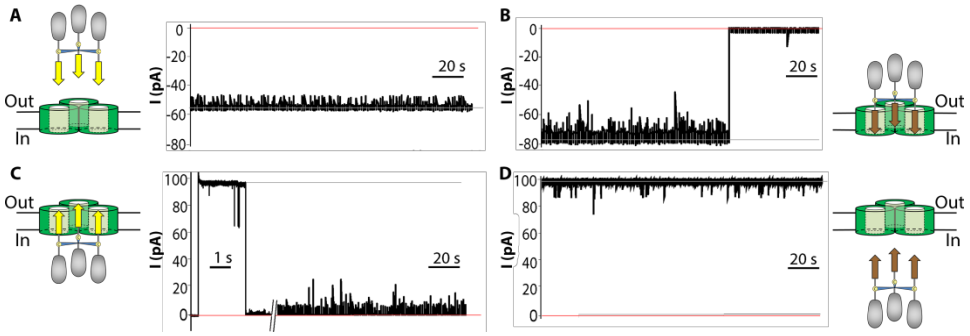

Figure 4. Voltage gated OmpF channels are occluded by $(OBS1)_3$ added from the periplasmic face of OmpF whilst $(OBS2)_3$ occludes from the extracellular face. Electrical recordings from single OmpF trimers incorporated into a DPhPC planar lipid bilayer with 50 nM $(OBS1)_3$ or $(OBS2)_3$ added to the *cis* compartment, corresponding to the extracellular side of the membrane (**A** and **B** respectively) were measured with a holding potential of -100 mV. Equivalent measurements adding 50 nM $(OBS1)_3$ or $(OBS2)_3$ to the trans chamber, corresponding to the periplasmic side of the membrane (**C** and **D** respectively) were made at a holding potential of +100 mV. For each experiment, channel recordings are shown over 3 min time courses, with the initial 4 sec shown on an expanded scale for the addition of $(OBS1)_3$ from the periplasmic side of the membrane, where the occlusion of OmpF channels was rapid. In each panel conductance of the open channel is marked with a grey line whilst the closed channel with zero conductance marked by a red line.

We further explored the directionality of OmpF binding by ColE9 OBSs through planar lipid bilayer (PLB) experiments. OmpF produces voltage-gated ion channels when inserted into PLBs and these channels have previously been shown to be inhibited by the addition of colicin fragments or OBS peptides(*8, 18, 19*), but the directionality of this inhibition has not been defined. Recently, the orientation of OmpF incorporated into planer lipid bilayers has been determined unambiguously through current-voltage asymmetry exhibited by the channels that are formed(*16*). We therefore investigated OBS1 and OBS2 binding to OmpF channels when added from either the periplasmic or extracellular side of the membrane. Tridentate ligands were used for these experiments rather than individual OBS peptides because of their higher affinity for OmpF and to minimise the possibility of translocation across the membrane. Addition of $(OBS1)_3$ to the extracellular side of OmpF in PLBs did not impact channel conductance, whilst addition to the periplasmic side occluded all three channels (**Figure 3**). In contrast, addition of $(OBS2)_3$ to the extracellular face blocked all three porin channels whereas

addition to the periplasmic face did not impact channel activity. We conclude that ColE9 OBS1 exhibits the same orientational bias for OmpF binding in PLBs as observed *in vivo* by fluorescence microscopy. Interestingly, the tridentate ligands showed simultaneous closure of all three pores, which once closed remain stably occluded, unlike the situation with the isolated OBS1 peptide where stepwise opening and closing of 1, 2 or 3 channels is observed(*8*). The absence of intermediate association states for the tridentate OBS ligands suggests their lifetimes must be significantly faster than the filter frequency of the PLB experiments (100 μs)(*20*). However, stepwise dissociation of the tridentate ligands from OmpF was observed when the potential was reversed (**Supplementary Figure 5**).The amino acid sequence of OBS1 not only encode OmpF binding but also dictate the peptide orientation within the lumen. In trying to rationalise the origin of direction-specific binding, one of the most notable differences between OBS1 and OBS2 is the length of the epitope, 17 and 10 residues, respectively. Given that the overall charge state of the two peptides is similar (~+2 at pH7), we truncated four residues from the N-terminus (OBS1) and created a tridentate ligand, assembled through reaction with TMEA as before and complexed with $Im9^{TMR}$. In contrast to $(OBS1)_3^{TMR}$, $\Delta^{2\text{-}5}$ $(OBS1)_3^{TMR}$ labelled B^E3000 cells without permeabilisation of the OM (**Figure 5**). As before, this labelling of cells was OmpF-dependent since BZB1107 cells were not labelled. Shortening OBS1 in $\Delta^{2\text{-}5}$ $(OBS1)_3^{TMR}$ removes the negatively charged aspartic acid from position 5. To ascertain whether shortening of OBS1 or removal of Asp5 facilitated binding of OBS1 from the outer face of OmpF, an Asp5-to-Ala5 mutation within OBS1 was generated within the context of a tridentate construct, D5A $(OBS1)_3^{TMR}$. This construct also labelled OmpF in intact cells without OM permeabilisation and blocked OmpF voltage-gated ion channels when added from the extracellular side of OmpF. These data were further corroborated by MD simulations of the $\Delta^{2\text{-}5}$ and D5A OBS1 peptide modelled with the N-terminus facing the periplasm both of which bound OmpF more stably than was observed for the wild-type sequence (**Figure 5**).

Contact analysis performed on MD simulations of the wild-type OBS1 shows that Asp5 interacted with various basic residues found around the periplasmic side of OmpF, but at the same time is repelled by negatively charged residues located adjacent to these basic residues, resulting in transient interactions (**Supplementary Figure 6**). The removal of Asp5 in D5A OBS1 mutant simulations produced more persistent contacts with OmpF, suggesting that the negatively charged N-terminus of OBS1 cannot bind strongly when approaching OmpF from the extracellular medium due to the presence of various acidic residues surrounding the porin eyelet. Since Asp5 in ColE9 serves such an important role in discriminating the orientation of OBS1 binding to OmpF pores we searched recently described nuclease bacteriocin sequences for evidence of N-terminal OBS1-type sequences. Remarkably, a highly conserved OBS1 sequence with a conserved aspartate at

position 5 is retained within the N-terminal disordered regions of nuclease bacteriocins produced by many species of *Enterobacteriaceae*, including *Klebsiella pneumoniae*, *Shigella sonnei*, *Salmonella enterica* and *Serratia marcescens* (**Supplementary Figure 7**). Sequence alignments of OmpF homologues from these species reveal conservation of the acidic residues responsible for the repulsion of Asp5 of OBS1 when binding from the extracellular face of OmpF (Supplementary Figure 8). We therefore conclude that all such OBS sequences will bind porins in the outer membranes of these organisms from the direction of the bacterial periplasm.

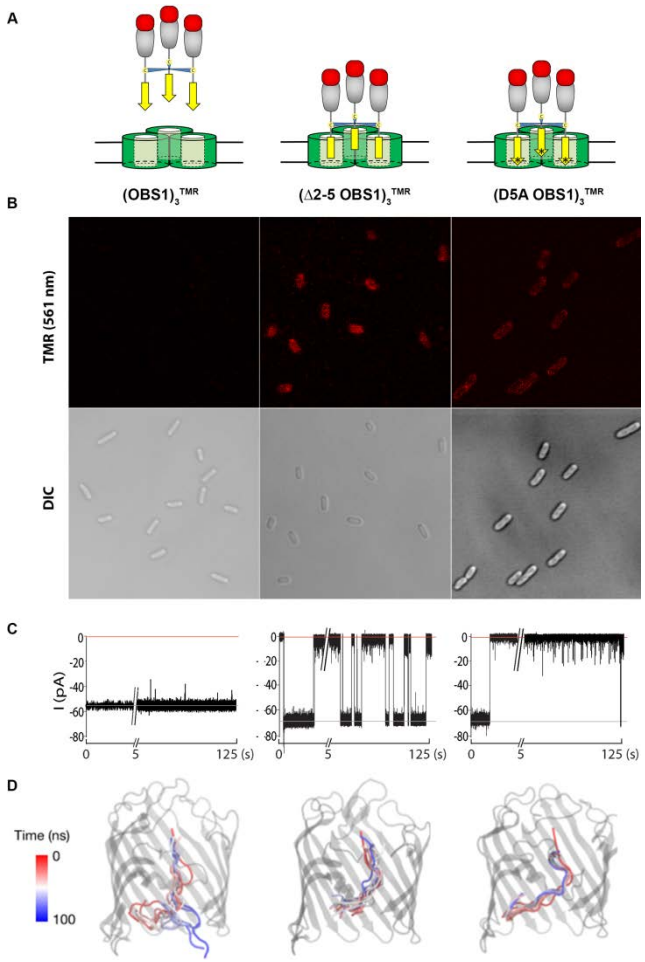

Figure 5. Negative charge within the N-terminus destabilises OBS1 interaction from the extracellular face of OmpF. **(A)** Cartoon representation of $(OBS1)_3^{TMR}$, $(\Delta 2\text{-}5\ OBS1)_3^{TMR}$ and $D5A\ OBS1)_3^{TMR}$ added to OmpF from the extracellular face. **(B)** Confocal fluorescence microscopy of $(OBS1)_3^{TMR}$, $(\Delta 2\text{-}5\ OBS1)_3^{TMR}$ and $(D5A\ OBS1)_3^{TMR}$ added to *E. coli* B^E3000 in the absence of permeabilisation of the outer membrane. Quantification of fluorescence intensities are shown in Supplementary Figure 4. **(C)** Electrical recording of single OmpF trimers incorporated into DPhPC planar lipid bilayers with $(OBS1)_3$, $(\Delta 2\text{-}5\ OBS1)_3$ and $(D5A\ OBS1)_3$ added to the *cis* (extracellular) chamber at a holding potential of -100 mV. Data are shown over 125 sec time courses with the

initial 5 sec shown on an expanded scale. Open channel conductance is marked with a grey line, whilst zero conductance is marked by the red line. **(D)** MD simulations for the OmpF·OBS1, OmpF·Δ2-5 OBS1 and OmpF·D5A OBS1 complexes with the N-terminus of the peptide modelled facing the periplasm, showing snap shots of the simulation over the 100 ns time course.

CONCLUSIONS

In summary, colicins such as ColE9 deploy their IUTDs once bound to their receptors on the OM of *E. coli*. MD simulations, fluorescence microscopy and single channel measurements using PLBs all show OBS1 at the extreme N-terminus of the ColE9 IUTD binds the OmpF lumen stably only when entering from the periplasmic side of the porin. This requires ~60 residues of the IUTD to translocate through a single OmpF monomer, by a passive process the mechanism of which has yet to be defined. Pre-concentration of the colicin onto the surface of the target bacterium is likely essential for this process to occur efficiently, with no interaction observed for OBS1 at the extracellular face of OmpF in either fluorescence microscopy or planar lipid bilayer experiments. Once translocated, both OBS1 (from the periplasm) and OBS2 (from the extracellular environment) bind different OmpF subunits within the same trimer, simultaneously locking the TBE in position within the *E. coli* periplasm in preparation for engagement with the energized TolQRA IM complex. Bioinformatics searches show that directional porin binding is likely to be common to the entry mechanisms of bacteriocins.

Previously the D5A mutation within OBS1 has been shown to reduce the affinity of OmpF binding by approximately 50-fold(7). Despite this loss in affinity, the same mutation within full length ColE9 surprisingly has no detrimental impact upon toxicity. Whilst this mutation weakens interaction with OmpF, its new binding site is now readily accessible on the outside of the target bacterium. This may assist transit of the TBE into the periplasm through a ratchet like mechanism, with initial low affinity interaction of OBS1 at the outer surface of OmpF aiding the threading of the IUTD through the OmpF pore, before being replaced by the higher affinity OBS2.

ASSOCIATED CONTENT

Supporting Figures S1-8. This material is available free of charge via the Internet at http://pubs.acs.org.

AUTHOR INFORMATION

Corresponding Author

*colin.kleanthous@bioch.ox.ac.uk

Present Addresses

† Laboratoire de Bioimagerie et Pathologie, UMR 7021, CNRS, Université de Strasbourg, Faculté de pharmacie, 74 Route du Rhin, 67401 Illkirch, France

Author Contributions

All authors have given approval to the final version of the manuscript.

Funding Sources

C.K., H.B. and S.K. acknowledge BBSRC for funding (BB/L021234/1 and BB/M020573/1). This work was also supported by a Wellcome Trust collaborative award to C.K. (201505/Z/16/Z).

ABBREVIATIONS

Colicin E9, ColE9; intrinsically unstructured translocation domain of ColE9, IUTD; OmpF binding site 1 (OBS1), OmpF binding site 2 (OBS2); TolB binding epitope, TBE; outer membrane, OM; inner membrane, IM; endonuclease, DNase; tetramethyl rhodamine, TMR; tris(2-maleimidoethyl)amine, TMEA TMEA-mediated tridentate OBS1 in the form of a colicin DNase fusion, $(OBS1)_3$; TMEA-mediated tridentate OBS1 in the form of a colicin DNase fusion with $Im9^{TMR}$ bound, $(OBS1)_3^{TMR}$; TMEA-mediated tridentate OBS2 in the form of a colicin DNase fusion, $(OBS2)_3$; TMEA-mediated tridentate OBS2 in the form of a colicin DNase fusion with $Im9^{TMR}$ bound, $(OBS2)_3^{TMR}$; planar lipid bilayers, PLBs; molecular dynamics, MD; isothermal titration calorimetry, ITC; n-octyl-β-D-glucopyranoside, β-OG.

REFERENCES

1. Nikaido, H. (2003) Molecular basis of bacterial outer membrane permeability revisited, *Microbiology and Molecular Biology Reviews 67*, 593-656.

2. Pages, J. M., James, C. E., and Winterhalter, M. (2008) The porin and the permeating antibiotic: a selective diffusion barrier in Gram-negative bacteria, *Nat Rev Microbiol 6*, 893-903.

3. Cascales, E., Buchanan, S. K., Duché, D., Kleanthous, C., Lloubès, R., Postle, K., Riley, M., Slatin, S., and Cavard, D. (2007) Colicin biology, *Microbiol Mol Biol Rev 71*, 158-229.

4. Majeed, H., Gillor, O., Kerr, B., and Riley, M. A. (2011) Competitive interactions in Escherichia coli populations: the role of bacteriocins, *ISME J 5*, 71-81.

5. Nedialkova, L. P., Denzler, R., Koeppel, M. B., Diehl, M., Ring, D., Wille, T., Gerlach, R. G., and Stecher, B. (2014) Inflammation fuels colicin Ib-dependent competition of *Salmonella* serovar *Typhimurium* and *E. coli* in enterobacterial blooms, *PLoS Pathog 10*, e1003844.

6. Sharp, C., Bray, J., Housden, N. G., Maiden, M. C. J., and Kleanthous, C. (2017) Diversity and distribution of nuclease bacteriocins in bacterial genomes revealed using Hidden Markov Models, *PLoS Comput Biol 13*, e1005652.

7. Housden, N. G., Wojdyla, J. A., Korczynska, J., Grishkovskaya, I., Kirkpatrick, N., Brzozowski, A. M., and Kleanthous, C. (2010) Directed epitope delivery across the Escherichia coli outer membrane through the porin OmpF, *Proceedings of the National Academy of Sciences of the United States of America 107*, 21412-21417.

8. Housden, N. G., Hopper, J. T., Lukoyanova, N., Rodriguez-Larrea, D., Wojdyla, J. A., Klein, A., Kaminska, R., Bayley, H., Saibil, H. R., Robinson, C. V., and Kleanthous, C. (2013) Intrinsically disordered protein threads through the bacterial outer-membrane porin OmpF, *Science 340*, 1570-1574.

9. Kleanthous, C. (2010) Swimming against the tide: progress and challenges in our understanding of colicin translocation, *Nat Rev Microbiol 8*, 843-848.

10. Wallis, R., Moore, G. R., James, R., and Kleanthous, C. (1995) Protein-protein interactions in colicin E9 DNase-immunity protein complexes. 1. Diffusion-controlled association and femtomolar binding for the cognate complex, *Biochemistry 34*, 13743-13750.

11. Vankemmelbeke, M., Zhang, Y., Moore, G. R., Kleanthous, C., Penfold, C. N., and James, R. (2009) Energy-dependent immunity protein release during *tol*-dependent nuclease colicin translocation, *J Biol Chem 284*, 18932-18941.

12. Yamashita, E., Zhalnina, M. V., Zakharov, S. D., Sharma, O., and Cramer, W. A. (2008) Crystal structures of the OmpF porin: function in a colicin translocon, *The EMBO journal 27*, 2171-2180.

13. Stansfeld, P. J., Goose, J. E., Caffrey, M., Carpenter, E. P., Parker, J. L., Newstead, S., and Sansom, M. S. (2015) MemProtMD: Automated Insertion of Membrane Protein Structures into Explicit Lipid Membranes, *Structure 23*, 1350-1361.

14. Delano, W. L. (2002) The PyMOL Molecular Graphics System, *DeLano Scientific, Palo Alto, CA, USA*.

15. Maglia, G., Heron, A. J., Stoddart, D., Japrung, D., and Bayley, H. (2010) Analysis of single nucleic acid molecules with protein nanopores, *Methods Enzymol 475*, 591-623.

16. Ionescu, S. A., Lee, S., Housden, N. G., Kaminska, R., Kleanthous, C., and Bayley, H. (2017) Orientation of the OmpF Porin in Planar Lipid Bilayers, *Chembiochem : a European journal of chemical biology 18*, 554-562.

17. Rassam, P., Copeland, N. A., Birkholz, O., Toth, C., Chavent, M., Duncan, A. L., Cross, S. J., Housden, N. G., Kaminska, R., Seger, U., Quinn, D. M., Garrod, T. J., Sansom, M. S., Piehler, J., Baumann, C. G., and Kleanthous, C. (2015) Supramolecular assemblies underpin turnover of outer membrane proteins in bacteria, *Nature 523*, 333-336.

18. Kurisu, G., Zakharov, S. D., Zhalnina, M. V., Bano, S., Eroukova, V. Y., Rokitskaya, T. I., Antonenko, Y. N., Wiener, M. C., and Cramer, W. A. (2003) The structure of BtuB with bound colicin E3 R-domain implies a translocon, *Nature Structural Biology 10*, 948-954.

19. Zakharov, S. D., Eroukova, V. Y., Rokitskaya, T. I., Zhalnina, M. V., Sharma, O., Loll, P. J., Zgurskaya, H. I., Antonenko, Y. N., and Cramer, W. A. (2004) Colicin occlusion of OmpF and TolC channels: Outer membrane translocons for colicin import, *Biophys J 87*, 3901-3911.

20. Qing, Y., Pulcu, G. S., Bell, N. A. W., and Bayley, H. (2018) Bioorthogonal Cycloadditions with Sub-Millisecond Intermediates, *Angewandte Chemie 57*, 1218-1221.

For Table of Contents Only